PNNL-27835

Pacific Northwest NATIONAL LABORATORY

NDE Technology Development Program for Hanford DST Non-Visual Volumetric Inspection Technology – Phase II

Technical Letter Report on Air-slot NDE Sensor Maturation Testing

August 2018

Traci L. Moran
Michael R. Larche
Kayte M. Denslow
S. W. (Bill) Glass

U.S. DEPARTMENT OF ENERGY

Prepared for the U.S. Department of Energy
under Contract DE-AC05-76RL01830

PACIFIC NORTHWEST NATIONAL LABORATORY
operated by
BATTELLE
for the
UNITED STATES DEPARTMENT OF ENERGY
under Contract DE-AC05-76RL01830

Printed in the United States of America

Available to DOE and DOE contractors from the
Office of Scientific and Technical Information,
P.O. Box 62, Oak Ridge, TN 37831-0062;
ph: (865) 576-8401
fax: (865) 576-5728
email: reports@adonis.osti.gov

Available to the public from the National Technical Information Service
5301 Shawnee Rd., Alexandria, VA 22312
ph: (800) 553-NTIS (6847)
email: orders@ntis.gov <http://www.ntis.gov/about/form.aspx>
Online ordering: http://www.ntis.gov

This document was printed on recycled paper.

(8/2010)

PNNL-27835

NDE Technology Development Program for Hanford DST Non-Visual Volumetric Inspection Technology – Phase II

Technical Letter Report on Air-slot NDE Sensor Maturation Testing

August 2018

Traci L. Moran
Michael R. Larche
Kayte M. Denslow
S. W. (Bill) Glass

Prepared for
the U.S. Department of Energy
under Contract DE-AC05-76RL01830

Pacific Northwest National Laboratory
Richland, Washington 99352

Executive Summary

The Non-destructive Evaluation (NDE) Technology Development Program for non-visual (volumetric) inspection technology is designed to identify, down-select, and mature volumetric NDE sensor technology and robotic deployment technology for Hanford double-shell tank (DST) systems. The program is currently focused on NDE technology for primary tank bottom inspection and comprised of three phases that will culminate in robotic NDE inspection systems that are qualified to assess the leak integrity of primary tank bottoms and operate under DST environmental conditions. Phase I of the NDE Non-visual Technology Development program screened, tested, and evaluated candidate ultrasonic NDE sensor technologies and culminated with the selection of two complementary sensor technologies—an ultrasonic guided wave phased-array (GWPA) air-slot NDE sensor and a remote electromagnetic acoustic transducer (EMAT) guided-wave NDE sensor. Phase II of the program was initiated in January 2018 and has focused initially on the maturation of the GWPA air-slot NDE sensor technology.

Significant progress was made in FY 2018 on the maturation of the GWPA air-slot NDE sensor technology through the completion of air-slot NDE sensor designs, fabrication of the first air-slot NDE sensor tailored for primary tank bottom inspection from refractory pad air-slots, and the start of testing to objectively demonstrate whether the sensor meets Phase II flaw detection requirements for NDE sensors.

The first GWPA air-slot NDE sensor—"Hanford-Probe A"—was designed by Guidedwave (Bellefonte, Pennsylvania) and fabricated by Olympus America Inc. (Waltham, Massachusetts). The flaw detection performance of "Hanford-Probe A" was demonstrated by Guidedwave in August 2018 at the Pacific Northwest National Laboratory (Richland, Washington). Testing was conducted to satisfy Phase II Flaw Detection Performance Tests for the sensor, which are designed to (1) demonstrate the extent to which flaw detection requirements are satisfied, (2) uncover any flaw detection performance deficiencies, and (3) identify any necessary sensor design improvements that would improve flaw detection performance.

Phase II Flaw Detection Performance Tests with Hanford-Probe A were conducted on primary tank test mock-ups that are constructed with plate thicknesses, carbon steel plate material, welds, and surface conditions that are representative of those found in the primary tanks of the AZ/SY/AW/AN/AP tank farms. The primary tank mock-ups contain surrogate corrosion pits, weld seam openings/cracks, and gradual wall thinning (general corrosion) to represent the primary degradation mechanisms of concern in Hanford tanks. The surrogate flaws are present in the test mock-up plates and welds in a range of flaw sizes that include reportable-level and U.S. Department of Energy actionable-level flaw sizes.

The scope of the tests summarized in this report are those which were conducted to facilitate a comparison of Hanford-Probe A flaw detection performance with the flaw detection performance of the original GWPA NDE sensor demonstrated under Phase I, which served as the basis for selecting the sensor technology for maturation. The results from the performance comparison demonstrate that the flaw detection capability of Hanford-Probe A is equivalent to that of the original GWPA sensor. Similar to the original GWPA sensor, Hanford-Probe A has the ability to detect surrogate corrosion pits with depths of 25% wall thickness and greater, surrogate weld seam openings/cracks with depths of 20% wall thickness and greater, and gradual wall thinning with depths of 50% wall thickness and greater. Another notable outcome of testing, which will affect the robotic deployment system, is the dry couplant material used with "Hanford-Probe A" requires a coupling force of approximately 150 lb.

A design improvement that should be made to Hanford-Probe A to further optimize its flaw detection performance is to achieve an ultrasonic center frequency closer to the design target frequency of 150 kHz in order to (1) maximize the send/receive efficiency of the piezoelectric rings and (2) minimize the generation of undesirable sound beam side lobes and wave-mode dispersion that reduce signal fidelity.

Acronyms and Abbreviations

DOE	U.S. Department of Energy
DST	double-shell tank
EMAT	electromagnetic acoustic transducer
GWPA	Guidedwave phased array
ID	identification
NDE	non-destructive evaluation
PII	Phase II (in context of mock-up)
PNNL	Pacific Northwest National Laboratory
SET	Sensor Effectiveness Testing
SNR	signal-to-noise ratio
TS	technology screening
WRPS	Washington River Protection Solutions

Contents

Executive Summary ii
Acronyms and Abbreviations iii
1.0 Introduction 1
2.0 Background 1
3.0 Scope 2
3.1 Phase II Scope of Testing 2
3.2 Scope of Phase II Testing Reported 3
4.0 Test Description 4
4.1 Mock-ups 4
4.2 Surrogate Flaws 7
4.3 Test Conditions 10
5.0 Methods 12
5.1 Phase I (FY 2017) 12
5.2 Phase II (FY 2018) 13
6.0 Results and Discussion 16
6.1 Overall Flaw Detection Summary 16
6.2 Flaw Type – Pit (P4) 17
6.3 Flaw Type – Notch (N4) 20
6.4 Flaw Type – Wall Thinning 21
6.5 Testing Challenges 24
7.0 Conclusions 24
8.0 Future Work 25
9.0 References 26

Figures

Figure 1. Summary of NDE Technology Development Program 2

Figure 2. Diagram Illustrating the Hierarchy and Organization of Flaw Detection Performance Tests and Their Relation to Type of Test Flaws. The natural progression of flaw detection performance tests is indicated by the arrows. 4

Figure 3. Isometric View of the TS Mock-up (*top)*; Isometric View of the PII Mock-up (*bottom*). Flaws circled in red are the test flaws used to facilitate the flaw detection performance comparison between new GWPA air-slot NDE sensor Hanford-Probe A and the original GWPA sensor demonstrated in FY 2017. 6

Figure 4. Top-down View Drawings of the TS Mock-up (top) and SET Mock-up (bottom) with Sensor Location Labels 11

Figure 5. The GWPA Sensors Used during FY 2017 Phase I Testing 12

Figure 6. GWPA Inspection Locations on the 1/2-inch-thick Bottom Plate of the *SET* Mock-up during the FY 2017 Phase I test campaign *Sensor Effectiveness Testing* 13

Figure 7. (a) Hanford-Probe A with 26 Elements in Elliptical Pattern, (b) Hanford-Probe A in Magnetic Coupler, (c) Hanford-Probe A with 150 ft. of Cable, and (d) Hanford-Probe A in Magnetic Coupler Interrogating the PII Mock-up 15

Figure 8. Photograph of Pit P4 17

Figure 9. GWPA Scan on the *SET* Mock-up at Location C, Collected at 160 kHz with the Original GWPA Sensor (image from Figure 40 of Appendix A in Moran et al. 2017b) 18

Figure 10. Composite Image from the *SET* Mock-up, Collected From 13 Measurement Locations with the Original GWPA Sensor (Figure 26 of Appendix A in Moran et al. 2017b) 18

Figure 11. GWPA Scan on the PII Mock-up, Collected at 150 kHz with Hanford-Probe A, Showing Detection of Surrogate Flaws P4, P8, P5, B1, T3, and B2 19

Figure 12. Composite Image from the PII Mock-up, Collected From Eight Measurement Locations with Hanford-Probe A 19

Figure 13. Photograph of Notch N4 20

Figure 14. Guidedwave GWPA Scan on the *SET* Mock-up at Location J, Collected at 160 kHz with the Original GWPA Sensor (image from Figure 22 of Appendix A in Moran et al. 2017b) 21

Figure 15. GWPA Scan on the PII Mock-up, Collected at 165 kHz with Hanford-Probe A, Showing Detection of Surrogate Flaws N4, P8, and B2 21

Figure 16. Photograph of Wall Thinning T3 22

Figure 17. GWPA Scan on the *SET* Mock-up at Location II, Collected at 225 kHz with the Higher Frequency Version of the Original GWPA Sensor Design (image from Figure 64 of Appendix A in Moran et al. 2017b) 23

Figure 18. GWPA Scan on the PII Mock-up, Collected at 195 kHz with Hanford-Probe A, Showing Detection of T3 and B1 (suppression filter turned off) 23

Tables

Table 1. Summary Flaw Matrix for *Maturation Testing: Phase II Capability Testing with Phase I Flaws* 7

Table 2. Subset of Phase II Capability Flaws used to Facilitate *Maturation Testing: Phase II Capability Testing with Phase I Flaws* 8

Table 3. Phase I Sensor Locations on *SET* and TS Mock-ups 10

Table 4. Comparison of Design Features between the Original GWPA Sensor and the New Air-slot GWPA Sensor "Hanford-Probe A" 14

Table 5. Summary Flaw Detection Table for Phase I and Phase II Comparison 16

1.0 Introduction

The Pacific Northwest National Laboratory (PNNL) located in Richland, Washington, hosted and administered Phase II Flaw Detection Performance Tests in August 2018 for a newly matured ultrasonic guided wave phased-array (GWPA) air-slot NDE sensor—"Hanford-Probe A." The purpose of testing was to evaluate the sensor for its flaw detection capability and repeatability.

A portion of the Phase II Flaw Detection Performance Tests was performed on a subset of test flaws on which the original GWPA sensor had been evaluated during Phase I *Sensor Effectiveness Testing* (*SET*). The results of testing on the flaw subset facilitated a comparison in flaw detection performance between Hanford-Probe A and the original GWPA sensor demonstrated in Phase I. The objective of the performance comparison was to determine the extent to which GWPA sensor design changes impacted the flaw detection performance upon which selection of the sensor technology was originally based. The purpose of the comparison was to determine whether the flaw detection performance of the newly matured Hanford-Probe A GWPA air-slot NDE sensor is at least equal to that of the original GWPA sensor evaluated under Phase I *SET*, or if design improvements are warranted to improve flaw detection performance.

This technical letter report presents the results produced by the new Hanford-Probe A on the Phase I test flaws and the results of the flaw detection performance comparison between Hanford-Probe A and the original GWPA sensor demonstrated in Phase I.

The remainder of this report is organized into nine sections. Section 2.0 summarizes the background on the double-shell tank (DST) Non-destructive Evaluation (NDE) Technology Development Program; Section 3.0 describes the scope of Phase II testing, the scope of testing completed in FY 2018, and the scope of this report; Section 4.0 describes the testing conducted to facilitate the sensor performance comparison; Section 5.0 describes the GWPA sensor technology used in Phase I and Phase II testing; Section 6.0 provides the results of the Hanford-Probe A testing and the comparison in performance between Hanford-Probe A and the original GWPA sensor; Section 7.0 provides conclusions; Section 8.0 discusses the future work needed to complete Phase II testing; and Section 9.0 presents the references cited throughout the technical letter report.

2.0 Background

In FY 2016, Washington River Protection Solutions (WRPS) began leading a NDE Technology Development Program designed to address the need for non-visual volumetric NDE technologies for DST primary tank bottom inspection. The goal of the program is to identify and mature one or more volumetric NDE technologies that can be transitioned to the DST Integrity Program to address non-visual volumetric inspection needs for primary tank bottoms identified in the 2015 DST Integrity Improvement Plan (Garfield et al. 2015). The NDE Technology Development Program consists of three phases that will:

1. perform baseline evaluations of current or emerging NDE volumetric inspection technologies to identify the strongest candidate(s) for flaw detection and flaw characterization in a mock-up of a primary tank;
2. mature the strongest candidate NDE volumetric inspection technologies by adapting transducer hardware and robotic deployment systems to overcome primary tank bottom access challenges; and

3. culminate in a system or set of integrated NDE volumetric inspection technologies for demonstration in a full-scale DST cold test (non-nuclear) platform, where both the ability to detect and characterize flaws and overcome primary tank access challenges will be tested.

The planned three-phased approach is summarized in Figure 1.

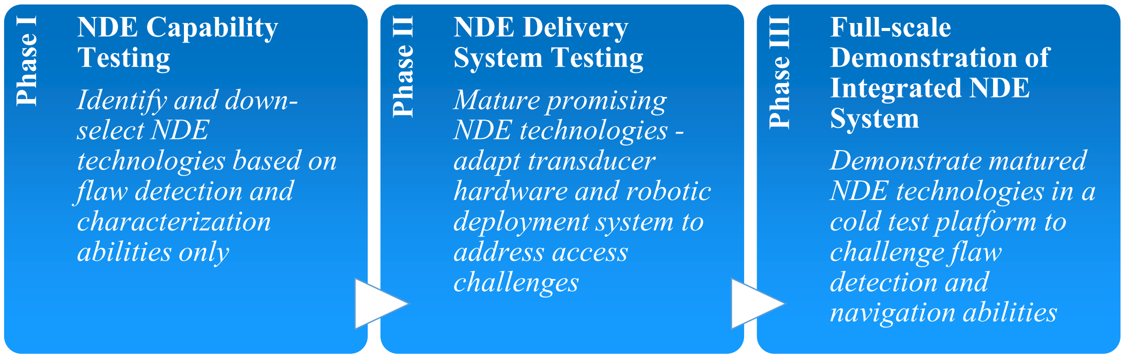

Figure 1. Summary of NDE Technology Development Program

Phase I of the NDE Technology Development Program began in FY 2017 and concluded in the first quarter of FY 2018. The first phase consisted of a series of laboratory tests to baseline the performance of current and emerging volumetric NDE technologies for their ability to detect and characterize primary tank bottom flaws in representative DST mock-ups. Four candidate NDE sensor technologies were evaluated that used ultrasonic guided-wave techniques to volumetrically examine areas around the sensors that extended over ranges of approximately 6 inches to over 14 feet, depending on the sensor. The full details of the test mock-ups, surrogate flaws, sensor technologies, evaluation criteria, and evaluation results are captured between the FY 2017 test reports (Moran et al. 2017a, b) and the FY 2018 final Phase I report (Denslow et al. 2018a). Phase I of the program culminated with the identification of a remote NDE sensor technology and an air-slot NDE sensor technology for adaptation and maturation under Phase II of the program.

The programmatic objective of Phase II is to mature both the remote and air-slot NDE sensors and their robotic deployment system counterparts to meet the subsystem requirements set forth in the Phase II requirements document "Phase II Technical Requirements for Sensor & Robotic Deployment System Maturation" (Denslow et al. 2018b). The purpose of Phase II is to properly prepare each NDE sensor and robotic deployment subsystem for future mechanical, electrical, and software integration.

3.0 Scope

This section summarizes the full scope of Phase II testing for the NDE Technology Development Program and describes the specific scope of Phase II testing addressed in this technical letter report.

3.1 Phase II Scope of Testing

Testing for the remote electromagnetic acoustic transducer (EMAT) NDE sensor subsystem, the ultrasonic GWPA air-slot NDE sensor subsystem, and the robotic deployment subsystems for each sensor type are included in the overall scope of Phase II testing. Phase II testing is intended for individual subsystems as they are each being matured to meet the requirements set forth in the Phase II requirements document.

The tests specified in the Phase II test plan are limited to those necessary to verify the satisfaction of a *subset* of the 20 standard, 23 NDE sensor, and 25 robotic deployment subsystem requirements in the Phase II requirements document for which testing was deemed the most appropriate verification method. Testing was selected as the appropriate verification method if it could be expected to provide the most efficient means for demonstrating requirement verification or if it was the only verification method that could be expected to provide objective evidence of requirement satisfaction. A majority of testing defined in the Phase II test plan will be performed in a non-nuclear (cold) test environment. A small number of tests will be performed in a facility with radiation sources (e.g., hot cells) to demonstrate sensor/robot functionality before, during or after exposure to gamma radiation.

Phase II testing supports the Phase II programmatic objective of completing maturation of the NDE sensor and robotic deployment subsystems. Maturation will be considered complete when testing or other appropriate verification methods identified in the Phase II test plan are completed and have generated objective evidence that each matured subsystem has the ability to satisfy all of its respective Phase II requirements.

3.2 Scope of Phase II Testing Reported

The GWPA air-slot NDE sensor Hanford-Probe A is the first sensor technology to undergo the maturation process and thus the scope of Phase II testing conducted in FY 2018 and the scope of this letter report pertain to Hanford-Probe A.

NDE sensor testing identified in the Phase II test plan is divided into nine different tests:

1. **Flaw Detection Performance**
2. Range
3. Positional Error Effects
4. Field Representative Surfaces
5. Effects of Tank Temperature
6. False Positives/False Calls
7. Consumable/Replacement Components
8. Radiation Tolerance
9. Humidity and Air Flow Tolerance

Flaw Detection Performance tests are regarded as high-priority tests to be performed early in the NDE sensor maturation process because they are designed to evaluate the extent to which the matured technologies satisfy their core functional and performance requirements, which are detection of degradation types and sizes of concern for high-level waste tanks.

Flaw Detection Performance tests are divided into two types of testing—Capability Testing with open test flaws and Repeatability Testing with blind test flaws. Capability Testing is designed to demonstrate the functionality of the NDE sensor when vendors have *a priori* knowledge of the type, quantity, size and location of the test flaws. The tests serve to verify the NDE sensor can meet flaw detection requirements, or reveal needs to improve sensor functionality through design improvement. Repeatability Testing is designed to demonstrate whether the NDE sensors are capable of providing the same level of performance demonstrated during Capability Testing, but without *a priori* knowledge of the type, quantity, size and location of the test flaws. The tests serve to demonstrate the level of flaw detection and reporting reliability that can be expected when true-state conditions are unknown (real-world scenarios).

The full scope of Capability Testing and an initial start on Repeatability Testing were completed for Hanford-Probe A in FY 2018. A portion of Capability Testing with Hanford-Probe A was satisfied by performing flaw detection tests on a subset of pre-existing test flaws from Phase I, which facilitated a flaw detection performance comparison between the new air-slot GWPA sensor Hanford-Probe A and the original GWPA sensor that had been demonstrated on the same subset of flaws during Phase I testing in FY 2017. The portion of Capability Testing performed with Hanford-Probe A on the subset of pre-existing Phase I test flaws is referred to as *Maturation Testing: Phase II Capability Testing with Phase I Flaws* in this technical letter report. Figure 2 attempts to illustrate the organization and hierarchy of the Flaw Detection Performance tests; the types of test flaws that support each test campaign (increment of testing); and how the *Maturation Testing* test campaign fits into the full scope of Flaw Detection Performance tests.

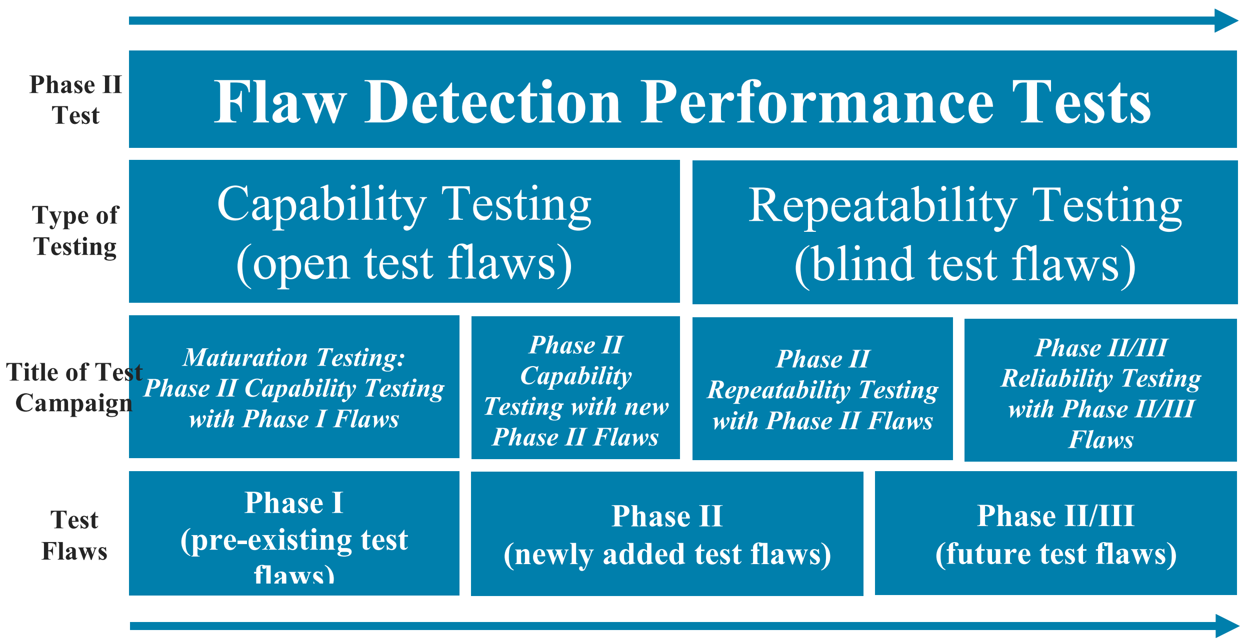

Figure 2. Diagram Illustrating the Hierarchy and Organization of Flaw Detection Performance Tests and Their Relation to Type of Test Flaws. The natural progression of flaw detection performance tests is indicated by the arrows.

4.0 Test Description

This section describes the primary tank test mock-ups, test flaws, and test conditions used to support *Maturation Testing: Phase II Capability Testing with Phase I Flaws*.

4.1 Mock-ups

Two primary tank test mock-ups were used to support *Maturation Testing: Phase II Capability Testing with Phase I Flaws.* Drawings of the mock-ups are provided in Figure 3 and are referred to here as the modified Technology Screening (TS) mock-up and new Phase II (PII) mock-up.

The plate thicknesses of both primary tank test mock-ups are representative of those found in 26 of the 27 in-service DSTs that are located in the AZ/SY/AW/AN/AP tank farms. The lower knuckle (curved plate) length and radius are also representative of those found in DST primary tanks. Each mock-up contains surrogate flaws that represent the primary degradation mechanism of concern in Hanford high-level waste tanks: pitting corrosion, general corrosion (wall thinning) and weld seam openings/cracks. The surrogate flaws in the primary tank test mock-ups are machined flaws with depths that span a range that includes actionable-level and reportable-level flaw sizes established for high-level waste tanks. Surrogate test flaws will be described in more detail in the subsequent section.

The new PII mock-up is 12 feet wide, 20 feet long, and constructed with A-516 Grade 70 carbon steel. Incorporated into the left side of the PII mock-up, as viewed in Figure 3, is the *SET* mock-up used in the FY 2017 Phase I test campaign *Sensor Effectiveness Testing* (Moran et al. 2017b). The *SET* portion of the PII mock-up that contains test flaws has a width of 6 feet and a length of 13 feet, where 10 feet are dedicated to 1/2-inch-thick mid-floor bottom plate and 3 feet are dedicated to 7/8-inch-thick plate. The width and length of the *SET* mock-up were selected to provide ample usable area in the mid-floor bottom plate to accommodate flaws with conservative 12-inch flaw spacing, and to accommodate a 1/2- to 1/2-inch weld pattern that may represent a high-risk area for flaw development—a 90-degree weld confluence found in the primary tank bottoms in the AY, AZ, and SY tank farms.

The modified TS mock-up is 4 feet wide, 12 feet long and constructed with A-516 Grade 70 carbon steel to represent the A-516 and A-515 carbon steel used in the construction of three of the six tank farms. Eight feet of mock-up length are dedicated to 1/2-inch-thick mid-floor bottom plate, three feet are dedicated to 7/8-inch-thick outer floor plate and one foot is dedicated to the 7/8-inch-thick rolled lower knuckle plate.

The 12-foot length of the modified TS mock-up represents approximately 90 percent of the distance from the outside lower knuckle of a DST to the first air-slot transition in the refractory pads upon which primary tanks rest for the AZ/SY/AW/AN/AP tank farms. The 20-foot length of the new PII mock-up covers the approximate 14-foot and 17-foot distances from the outside lower knuckle to the first air-slot transition in the refractory pads for the AZ/SY/AW/AN/AP tank farms and AY tank farm, respectively. Reaching the first air-slot transition is the first navigation goal for NDE volumetric inspection technologies that require direct contact with the exterior surface of the primary tank bottom.

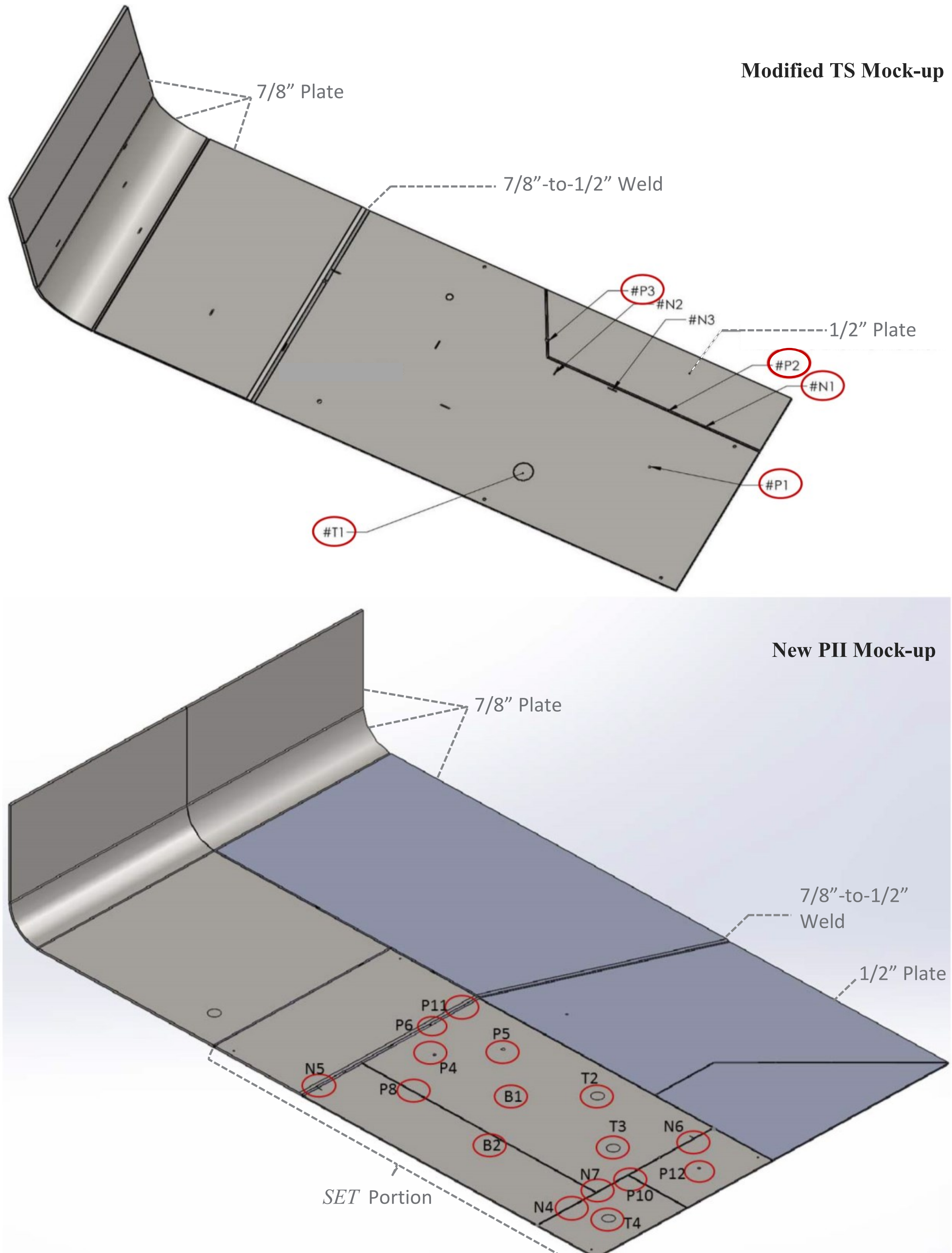

Figure 3. Isometric View of the TS Mock-up (*top)*; Isometric View of the PII Mock-up (*bottom*). Flaws circled in red are the test flaws used to facilitate the flaw detection performance comparison between new GWPA air-slot NDE sensor Hanford-Probe A and the original GWPA sensor demonstrated in FY 2017.

4.2 Surrogate Flaws

A subset of 21 surrogate flaws ("test flaws") identified in the Capability Testing flaw matrix in the Phase II test plan were used to support *Maturation Testing: Phase II Capability Testing with Phase I Flaws*. The surrogate flaws represent corrosion-type pitting, wall thinning, and weld seam openings/cracks. Flaw sizes for each of the three surrogate flaw types were selected to bound the conservative reportable-level values used by WRPS and the actionable-level values established for U.S. Department of Energy (DOE) high-level waste tanks (Bandyopadhyay et al. 1997). The reportable-level and actionable-level depths for each type of flaw, which represent thresholds for the response protocols described in Boomer et al. 2016, are indicated in Table 1. The depths of the test flaws used in *Maturation Testing: Phase II Capability Testing with Phase I Flaws* are indicated by yellow highlighted cells.

Table 1. Summary Flaw Matrix for *Maturation Testing: Phase II Capability Testing with Phase I Flaws*

	Flaw Type		
Flaw Depth	Pit	Crack[(a)]	Wall Thinning
10% plate thickness			Reportable Level
20% plate thickness		Reportable Level[(b)]	Actionable Level
25% plate thickness	Reportable Level		
50% plate thickness	Actionable Level	Actionable Level	
75% plate thickness			

(a) Criteria for cracks were also applied to weld seam openings.
(b) A 20% through-wall crack specified for the actionable-level value is equivalent to the 0.1-inch through-wall depth specified for the reportable-level value when flaw length is not a factor.

All pits inserted in the test mock-ups were machined with a diameter-to-depth ratio of 3:1. The machined notches that serve as surrogate weld separation/cracks are straight with lengths of 2.0 inch–3.0 inch, widths of 1/8 inch, and radius ends. Surrogate wall thinning is represented by a 4-inch-diameter thin-wall area with an ellipsoidal bottom and a maximum depth that match the target flaw depth. The detailed matrix of the subset of surrogate flaws that were used to support *Maturation Testing: Phase II Capability Testing with Phase I Flaws* is provided in Table 2. The flaw identifications (IDs) provided in the flaw matrix Table 2 correspond with the flaw IDs in the mock-up drawings in Figure 3.

A majority of the test flaws used in *Maturation Testing: Phase II Capability Testing with Phase I Flaws* are located in the *SET* portion of the new PII test mock-up in the 1/2-inch-thick base plate and the 1/2- to 1/2-inch welds up to and including the 1/2- to 7/8-inch transition weld. Two of the 16 surrogate flaws in the *SET* portion of the PII test mock-up (B1 and B2) originate from the bottom side plate of plate. The remaining five *Maturation Testing* test flaws are located in the modified TS mock-up in the 1/2-inch-thick base plate and the 1/2- to 1/2-inch welds up to and including the 1/2- to 7/8-inch transition weld. All five flaws originate from the top surface of the mock-up.

Although the *SET* mock-up was incorporated into the PII mock-up, the surrogate flaws featured in the *SET* portion of the mock-up were preserved during fabrication and thus not altered between Phase I and the start of Phase II *Maturation Testing*. The test flaws featured in the modified TS mock-up were also unaltered between FY 2017 Phase I testing and the start of FY 2018 Phase II *Maturation Testing*. Therefore, the set of 21 test flaws used to support the comparison of flaw detection performance between the original GWPA sensor and the new GWPA air-slot NDE sensor Hanford-Probe A can be expected to support a reliable comparison of flaw detection performance between the two sensors.

Table 2. Subset of Phase II Capability Flaws used to Facilitate *Maturation Testing: Phase II Capability Testing with Phase I Flaws*

	Flaw ID	Flaw Type	Flaw Depth (% Wall Thickness)	Actionable/ Reportable	Size	Location	Test Mock-up
1/2-in. Base Plate	P1	Pit	25% (0.13 in.)	Reportable	0.38 in. diameter	Base plate (top plate)	TS
	P4	Pit	50% (0.25 in.)	Actionable	0.75 in. diameter	Base plate (top plate)	PII-SET
	P5	Pit	75% (0.375 in.)	> Actionable	1.125 in. diameter	Base plate (top plate)	PII-SET
	B1	Pit	50% (0.25 in.)	Actionable	0.75 in. diameter	Base plate (bottom plate)	PII-SET
	P12	Pit	50% (0.25 in.)	Actionable	0.75 in. diameter	Base plate, located beyond a 1/2- to 1/2-in. weld (top plate)	PII-SET
	T1	Wall thinning	10% (0.050 in.)	Reportable	4.0-in. diameter	Base plate (top plate)	TS
	T2	Wall thinning	20% (0.10 in.)	Actionable	4.0 in. diameter	Base plate (top plate)	PII-SET
	T3	Wall thinning	50% (0.25 in.)	> Actionable	4.0 in. diameter	Base plate (top plate)	PII-SET
	T4	Wall thinning	50% (0.25 in.)	> Actionable	4.0 in. diameter	Base plate (top plate), located beyond a 1/2- to 1/2-in. weld	PII-SET
7/8–1/2 in. Weld	P11	Pit	25% (0.13 in.)	Reportable	0.38 in. diameter	7/8- to 1/2-in. transition weld (top plate)	PII-SET
	N5	Notch	50% (0.44 in.)	Actionable	2.0 in. long, 0.13 in. wide	7/8- to 1/2-in. transition weld (top plate), axial orientation, perpendicular to weld	PII-SET
	P6	Pit	50% (0.44 in.)	Actionable	0.75 in. diameter	7/8- to 1/2-in. transition weld (top plate)	PII-SET
1/2–1/2 in. Weld	P2	Pit	25% (0.13 in.)	Reportable	0.38 in. diameter	1/2- to 1/2-in. weld (top plate)	TS
	P8	Pit	50% (0.25 in.)	Actionable	0.75 in. diameter	1/2- to 1/2-in. weld (top plate)	PII-SET
	P10	Pit	50% (0.25 in.)	Actionable	0.75 in. diameter	1/2- to 1/2-in. weld (top plate), corner of 90° weld confluence	PII-SET
	P3	Pit	50% (0.25 in.)	Actionable	0.75 in. diameter	1/2- to 1/2-in. weld (top plate), within 30° angled weld	TS

Flaw ID	Flaw Type	Flaw Depth (% Wall Thickness)	Actionable/ Reportable	Size	Location	Test Mock-up
N1	Notch	20% (0.10 in.)	Reportable	2.0 in. long, 0.13 in. wide	1/2- to 1/2-in. weld (top plate), axial orientation, parallel with weld	TS
N4	Notch	50% (0.25 in.)	Actionable	2.0 in. long, 0.13 in. wide	1/2- to 1/2-in. weld (top plate), circumferential orientation, parallel with weld	PII-SET
N6	Notch	50% (0.25 in.)	Actionable	2.0 in. long, 0.13 in. wide	1/2- to 1/2-in. weld (top plate), axial orientation, perpendicular to weld	PII-SET
B2	Notch	50% (0.25 in.)	Actionable	3.0 in. long, 0.13 in. wide	1/2- to 1/2-in. weld (bottom plate), circumferential orientation, perpendicular to weld	PII-SET
N7	Notch	50% (0.25 in.)	Actionable	2.9 in. long, 0.13 in. wide	1/2- to 1/2-in. weld (top plate), extending from corner of 90° weld confluence, circumferential orientation, parallel with weld	PII-SET

4.3 Test Conditions

Maturation Testing: Phase II Capability Testing with Phase I Flaws was performed in a non-nuclear research laboratory test environment at PNNL in Richland, Washington. Volumetric examinations of the mock-up plates were performed by Guidedwave test personnel using Hanford-Probe A. Testing was conducted under an open format where all surrogate flaws were viewable during testing with the exception of Flaws B1 and B2 that originate from the underside of the *SET* portion of the new PII mock-up. The two flaws had supported early blind flaw testing during the FY 2017 Phase I test campaign *Sensor Effectiveness Testing.* Although the flaws were not viewable, the type and location of the two flaws were known by Guidedwave because they had been detected during Phase I testing in FY 2017.

Hanford-Probe A was placed on the top surface of the mock-ups during flaw detection testing because 1) the nature of the ultrasonic guided wave inspection method is not sensitive to flaw surface connectivity and 2) because it reduces the complexity associated with placing the sensor on the bottom surface of the mock-ups. The surfaces of the test mock-ups were coated with naturally occurring surface oxides throughout *Maturation Testing: Phase II Capability Testing with Phase I Flaws*.

In order to facilitate a fair comparison of flaw detection performance between GWPA air-slot NDE sensor Hanford-Probe A and the original GWPA sensor, Guidedwave was only permitted to place Hanford-Probe A on the same locations of the test mock-ups from which the data had been collected previously with the original GWPA sensor during Phase I testing. The list of reference locations on the two test mock-ups (PII and TS) is provided in Table 3. Drawings that illustrate the sensor measurement locations on the mock-ups are provided in Figure 4. The star on each mock-up drawing indicates the (0,0) origin.

Table 3. Phase I Sensor Locations on *SET* and TS Mock-ups

PII-*SET* Mock-up Locations	X (in)	Y (in)
A	21	55
AA	21	19
B	38	55
BB	21	3
C	56	55
CC	74	19
D	74	55
DD	74	3
E	21	37
F	38	37
G	56	37
H	74	37
I	11	11
J	29	11
K	47	11
L	65	11
M	83	11
N	101	28
P	114	19
R	101	46
S	114	55

TS Mock-up Locations	X (in)	Y (in)
EE	12	38
T	42	26
U	62	26
V	82	26
W	32	16
X	52	16
Y	72	16
Z	72	41

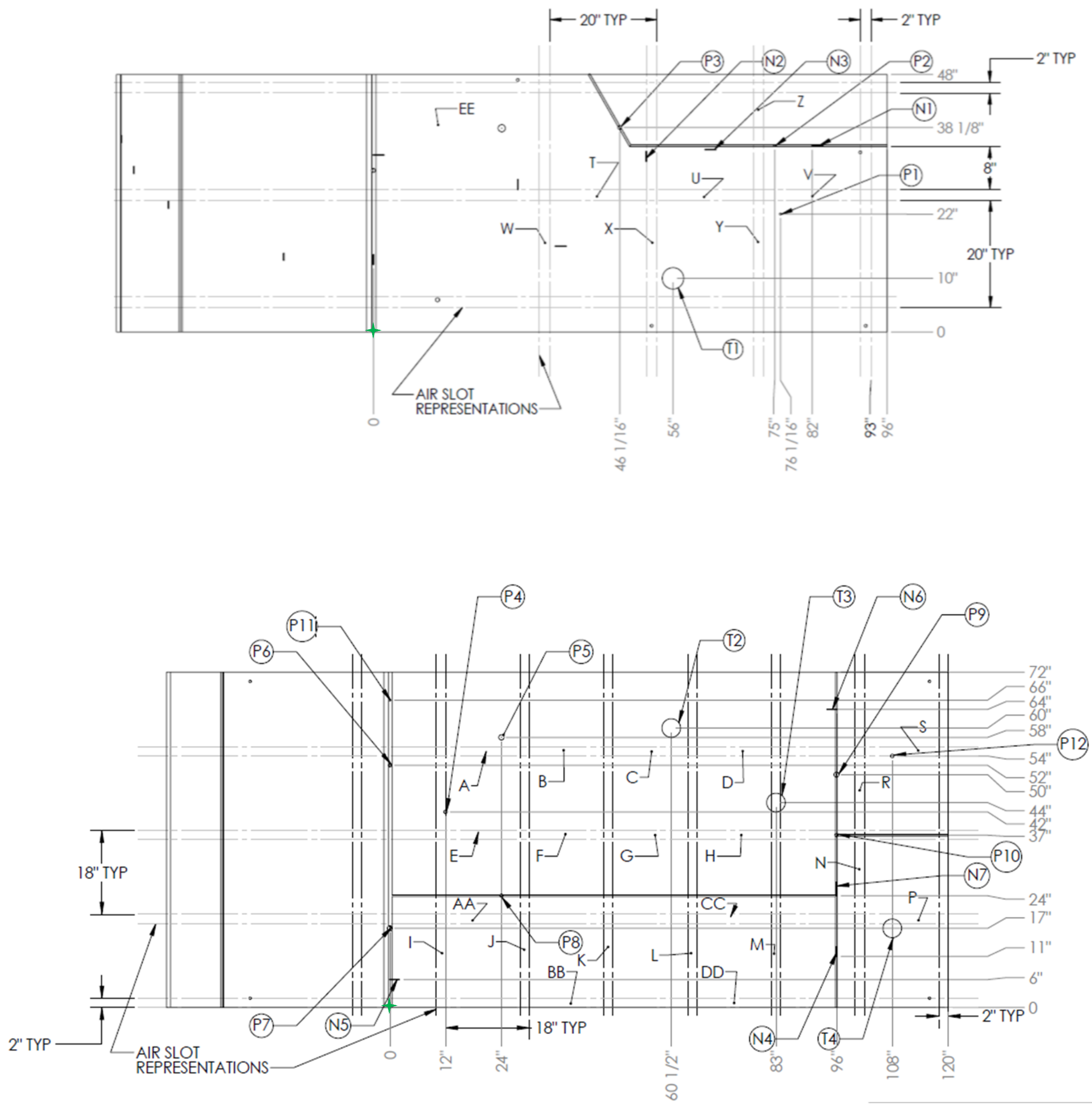

Figure 4. Top-down View Drawings of the TS Mock-up (top) and SET Mock-up (bottom) with Sensor Location Labels

5.0 Methods

This section describes the ultrasonic GWPA NDE sensors used during the FY 2017 Phase I test campaign *Sensor Effectiveness Testing* and the FY 2018 Phase II test campaign *Maturation Testing: Phase II Capability Testing with Phase I Flaws* for volumetric examination of the test mock-ups.

5.1 Phase I (FY 2017)

The flaw detection performance demonstration by Guidedwave during Phase I testing was performed using a volumetric examination method that utilizes ultrasonic shear-waves at specific ultrasonic frequencies to produce guided waves in the test plates that are responsible for flaw detection. The sensor technology that enables the examination is a single sensor containing a multitude of ultrasonic piezoceramic elements laid out in a pattern with spacings that are conducive to desired constructive and destructive interference. During sensor operation, specific time delays and excitation amplitudes are applied to a subset of piezoceramic elements in the array to produce a sound beam in a specific direction. The data acquisition instrumentation controls the time delays and applies them sequentially to different subsets of piezoceramic elements in the array to electronically steer the sound beam around the stationary GWPA sensor to inspect plate material 360° around the sensor.

The GWPA sensor used during Phase I required a liquid shear couplant to be applied to the sensor faceplate to facilitate the transfer of ultrasonic energy into the test material. The amount of force applied to the sensor to couple it properly was estimated to be less than 20 lbs. The two guided-wave sensors brought for Phase I *Sensor Effectiveness Testing* are shown in Figure 5.

Figure 5. The GWPA Sensors Used during FY 2017 Phase I Testing

Guidedwave selected a 165 kHz, 30-element GWPA sensor as the primary sensor with which to perform volumetric examinations of the test mock-ups. The active element portion of the transducer array, pictured on the right of Figure 5, is 2 inches in diameter and 3/8 inch in height and would be small enough to fit into the air-slots of a DST. The secondary sensor brought for testing was a 200 kHz, 30-element phased-array sensor with a diameter of 1.5 inches. The sensors were used to perform examinations of the 1/2-inch-thick bottom plate of the mock-ups. Multiple inspection locations on each plate allowed for post-processing of the data into a composite image. Figure 6 shows the Guidedwave participants and the equipment at an inspection location on the *SET* mock-up.

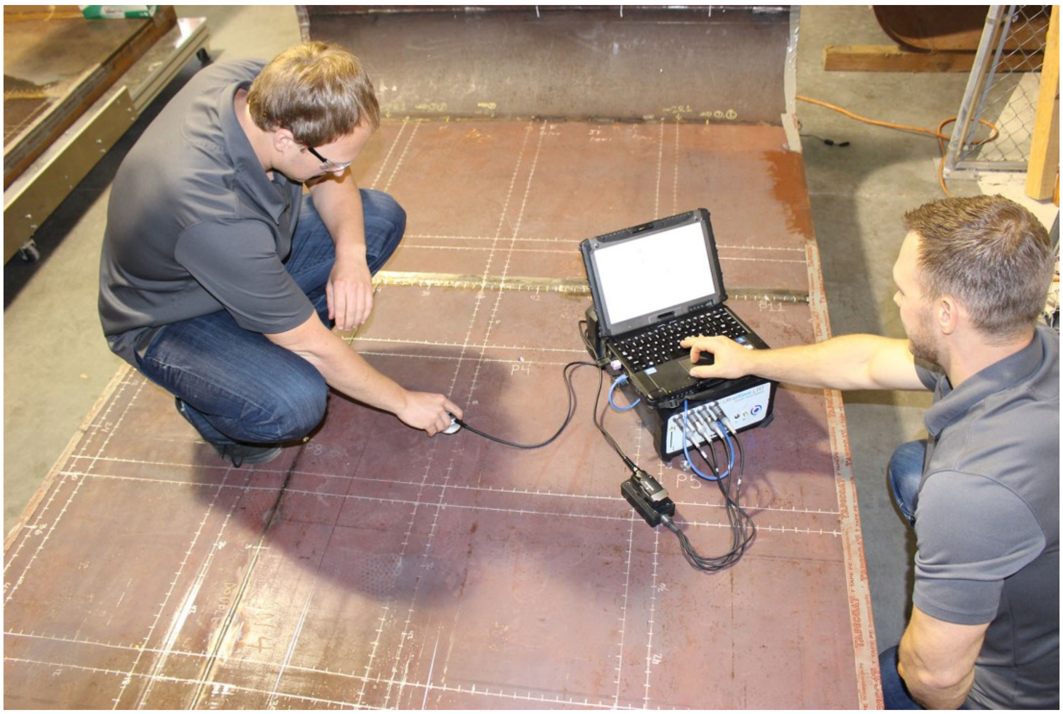

Figure 6. GWPA Inspection Locations on the 1/2-inch-thick Bottom Plate of the *SET* Mock-up during the FY 2017 Phase I test campaign *Sensor Effectiveness Testing*

5.2 Phase II (FY 2018)

During the FY 2018 Phase II test campaign *Maturation Testing: Phase II Capability Testing with Phase I Flaws*, the same ultrasonic guided-wave volumetric examination method was employed for flaw detection; however the GWPA sensor that was used for Phase II testing is an adapted version of the original GWPA sensor. The new GWPA sensor design still contains an array of piezoceramic elements that are used to inspect plate material 360° around the stationary sensor; however, the shape and size of the sensor housing was adapted in order to be co-located with an air-slot robotic deployment system in refractory pad air-slots during primary tank bottom inspections. A new ultrasonic center frequency was also targeted to further optimize the generation of non-dispersive shear waves over the range of tank plate thicknesses. The sensor housing modifications and ultrasonic frequency adjustment required changes in the size and array layout of the piezoceramic elements.

Guidedwave worked with their GWPA sensor manufacturer, Olympus, to redesign and build two different GWPA air-slot NDE sensors—"Hanford-Probe A" and "Hanford-Probe B." Hanford-Probe A was designed to be smaller and have a center frequency of 150 kHz. Hanford-Probe B was designed to have a center frequency of 120 kHz and be longer than Hanford-Probe A, but still within tolerances provided in the requirements document. Due to manufacturing delays, only Hanford-Probe A was available for FY 2018 Phase II testing. A comparison of the design features of Hanford-Probe A with the design features of the original GWPA sensor used in Phase I is provided in Table 4.

Hanford-Probe A (Figure 7(a)) was discovered to have a center ultrasonic frequency of 180–185 kHz during Phase II testing, which is approximately 20% higher than the target center frequency of 150 kHz. The higher ultrasonic frequencies in the mock-up plate thicknesses resulted in a prominent shear horizontal SH1 wave mode that is dispersive and interfered with the non-dispersive fundamental SH0 wave mode that is the intended wave mode for examination. The piezoceramic element layout and spacing for Hanford-Probe A, which were selected to be compatible with a center frequency of 150 kHz, resulted in sound beam side lobes that contributed to degraded signal fidelity. Guidedwave elected to operate Hanford-Probe A at discrete ultrasonic frequencies from 145 kHz up to 195 kHz throughout Phase II testing. When operating the 180-185 kHz sensor at the lower end of the frequency range closer to the desired center frequency (145–150 kHz), the piezoceramic elements responsible for sending/receiving ultrasonic energy are not as efficient, which resulted in lower amplitude responses.

Guidedwave is working with Olympus to determine the reasons for the high center frequency of Hanford-Probe A. The higher frequency is likely the result of getting a frequency down-shift magnitude that is different from that which typically results when free/undamped piezoceramic elements are placed into a sensor housing assembly and mechanically loaded (“damped”) with a backing material to control their bandwidth and secure them inside the sensor housing.

Table 4. Comparison of Design Features between the Original GWPA Sensor and the New Air-slot GWPA Sensor “Hanford-Probe A”

	Original GWPA Sensor	New Hanford-Probe A
Width	2.75 in.	1.5 in.
Length	2.75 in.	3.3 in.
Height	1.65 in.	<1.0 in.
Center Frequency	160 kHz	150 kHz (design) 180–185 kHz (actual)
Resolution Perpendicular to Major Axis	22 deg.	15 deg.
Resolution Perpendicular to Minor Axis	22 deg.	31.5 deg.
Average Side Lobe Amplitude	−26.9 dB	−21.9 dB
Elements	30	26
Shape	Circular	Elliptical
Coupling	“Wet” – Shear couplant direct contact with plate	“Dry” – Shear couplant in membrane (barrier layer between couplant and plate)
Application Force	<20 lbs.	>100 lbs.
Cable Length (between sensor and instrumentation)	8 ft.	>150 ft.

Guidedwave used a dry couplant membrane with Hanford-Probe A that places a non-adhesive layer between the shear couplant material and the test plates of the mock-ups. A dry couplant approach will avoid the use of a traditional liquid shear wave couplant and the complexities that would be associated with applying and removing a liquid couplant from primary tank bottom plates after each inspection.

However, the dry couplant membrane requires significantly more force to be applied to the sensor during an examination than that which was required when the original GWPA sensor was coupled with a liquid shear wave couplant. During Phase II testing with Hanford-Probe A, the force applied by the magnetic coupler (see Figure 7(b)) was determined to be slightly over 100 lbs., a force that was estimated by comparing the signal obtained with the magnetic coupler with signals obtained when weights were placed atop the sensor in 50-lb. increments. The improvement in signal amplitude and reduction of the "dead zone" around the sensor as a function of force led to a new recommended target sensor coupling force of 150 lb. The sensor coupling force will need to be provided by the robotic deployment system during primary tank bottom inspections.

When Hanford-Probe A was coupled to the test mock-ups with the dry couplant membrane and the ~100-lb. force supplied by the magnetic coupler, the dead zone immediately around the sensor was observed to have a radius of approximately 10 inches. The size of the dead zone is a function of the coupling force, sensor damping and instrument settings.

Figure 7 (c) shows the cable used with Hanford-Probe A, which was measured to be approximately 155 feet between the sensor and the data acquisition instrumentation. The cable length meets Requirement UT-15 from the Phase II requirements document. Figure 7(d) shows the Hanford-Probe A with the magnetic coupler on a primary tank mock-up during testing.

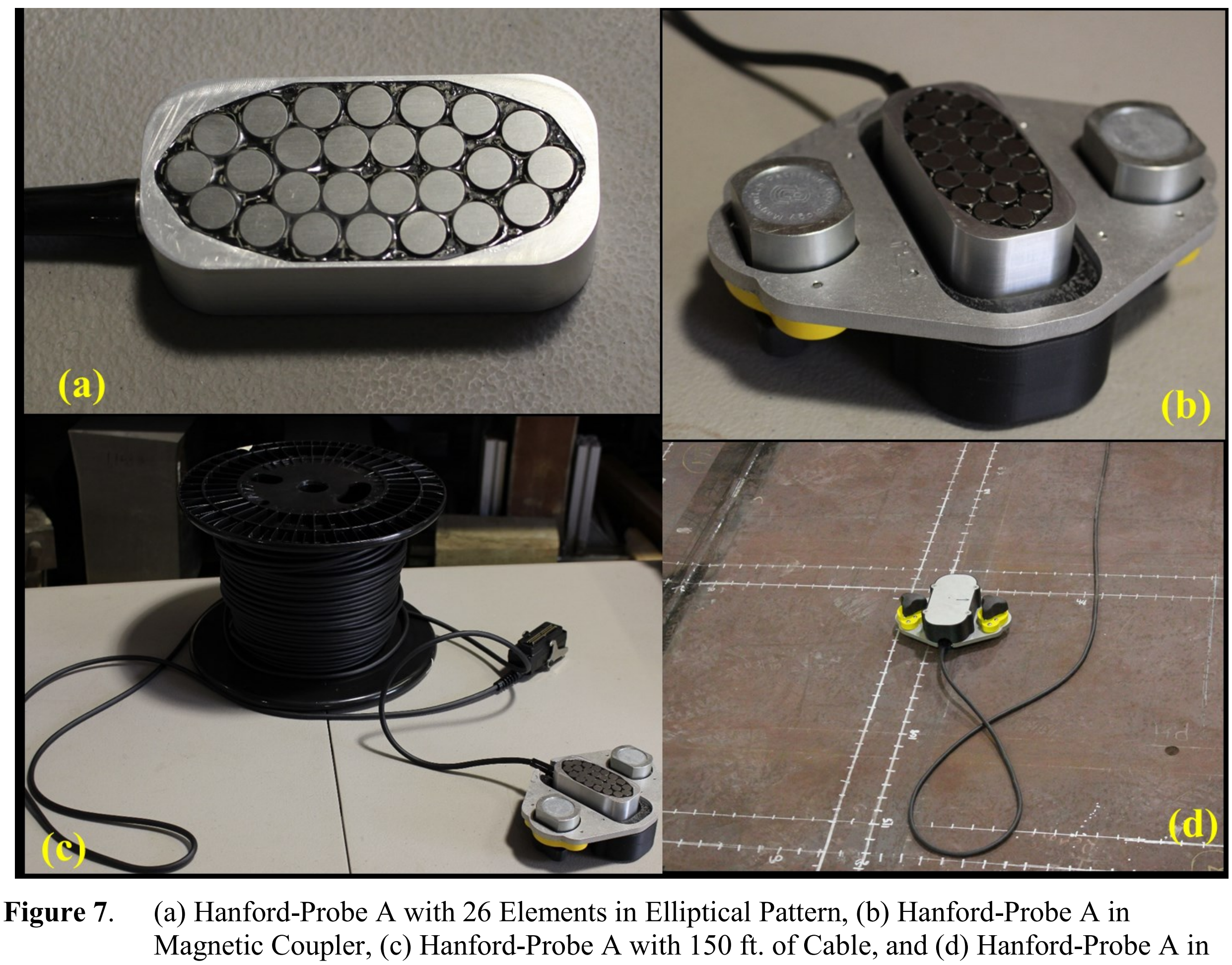

Figure 7. (a) Hanford-Probe A with 26 Elements in Elliptical Pattern, (b) Hanford-Probe A in Magnetic Coupler, (c) Hanford-Probe A with 150 ft. of Cable, and (d) Hanford-Probe A in Magnetic Coupler Interrogating the PII Mock-up

6.0 Results and Discussion

This section provides the flaw detection results obtained with Hanford-Probe A on the 21 surrogate flaws listed in Table 2 and the results of the flaw detection performance comparison between Hanford-Probe A and the original GWPA sensor demonstrated in FY 2017. Section 6.1 provides a summary table of the flaw detection results for both the original GWPA sensor (Phase I) and new GWPA air-slot NDE sensor Hanford-Probe A (Phase II) designs. Examples of data images for three different surrogate flaw types (pits, notches, and wall thinning) generated by the GWPA sensors are provided for comparison in Sections 6.2 through 6.4. Noteworthy observations made during *Maturation Testing: Phase II Capability Testing with Phase I Flaws* are listed in Section 6.5. Details on each of the 21 surrogate flaws and the full set of test results generated with the original GWPA sensor for the flaws during the Phase I test campaign *Sensor Effectiveness Testing* are provided in Moran et al. 2017b.

6.1 Overall Flaw Detection Summary

Table 5 provides a yes/no detection summary for the original Phase I GWPA sensor and the new Phase II GWPA air-slot NDE sensor Hanford-Probe A. The detection summary shows the original GWPA sensor detected all pits, notches, and both 50% deep wall-thinning flaws, but missed the 10% and 20% deep wall-thinning flaws. Hanford-Probe A also detected all pits and notches, but detected only one of the 50% deep wall-thinning flaws (T3); the other 50% deep wall-thinning flaw (T4) was missed due to reasons provided in Section 6.4. Both sensors were unable to detect 10% or 20% deep wall-thinning flaws.

Table 5. Summary Flaw Detection Table for Phase I and Phase II Comparison

Machined Surrogate Flaw	Flaw ID	Phase I (Y/N)	Phase II (Y/N)
Pit 25% Base Plate	P1	Y	Y
Pit 25% 1/2- to 1/2-in. Weld	P2	Y	Y
Pit 50% 1/2- to 1/2-in. Weld	P3	Y	Y
Pit 50% Base Plate	P4	Y	Y
Pit 75% Base Plate	P5	Y	Y
Pit 50% Transition Weld	P6	Y	Y
Pit 50% 1/2- to 1/2-in. Weld	P8	Y	Y
Pit 50% Pinwheel	P10	Y	Y
Pit 25% Transition	P11	Y	Y
Pit 50% Base Plate, Post-Weld	P12	Y	Y
Pit 50% Base Plate (Bottom)	B1	Y	Y
Notch 20% 1/2- to 1/2-in. Weld, Parallel	N1	Y	Y
Notch 50% 1/2- to 1/2-in. Weld, Parallel	N4	Y	Y
Notch 50% Transition Weld, Perpendicular	N5	Y	Y
Notch 50% 1/2- to 1/2-in. Weld, Perpendicular	N6	Y	Y
Notch 50% Pinwheel, Parallel	N7	Y	Y
Notch 50% 1/2- to 1/2-in. Weld, Perpendicular (Bottom)	B2	Y	Y
Wall Thinning 10% Base Plate	T1	N	N
Wall Thinning 20% Base Plate	T2	N	N
Wall Thinning 50% Base Plate	T3	Y	Y
Wall Thinning 50% Base Plate Post-Weld	T4	Y	**N**[1]

[1] For explanation in differences, see Section 6.4.

6.2 Flaw Type – Pit (P4)

Flaw P4 is a 0.750-inch-diameter pit with a depth of 50% of the plate thickness (0.250 in.) located in the base plate of the PII mock-up 12 inches from the 7/8- to 1/2-inch transition weld. A photograph of P4 is shown in Figure 8.

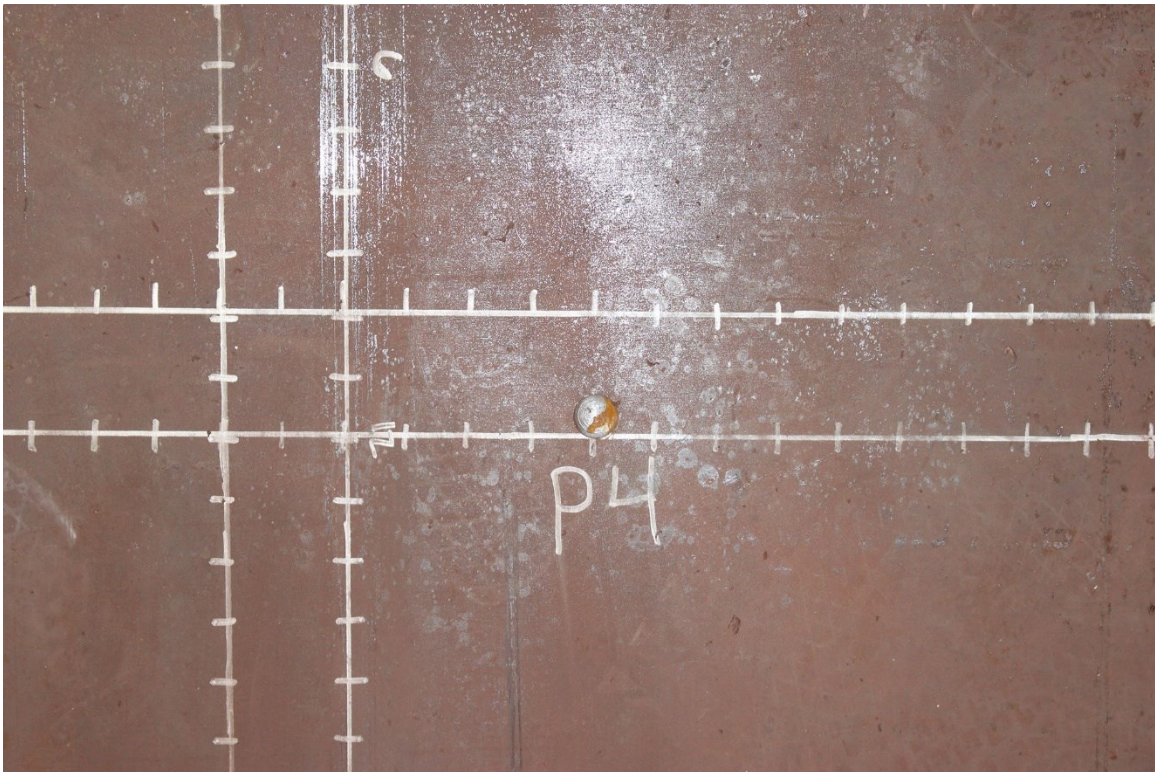

Figure 8. Photograph of Pit P4

Pit P4 was detected during FY 2017 Phase I testing with the original GWPA sensor and by the new GWPA sensor Hanford-Probe A during FY 2018 Phase II testing.

In Phase I, Guidedwave detected P4 from four different transducer locations at an excitation frequency of 160 kHz. Transducer Location C was the farthest from Pit P4 at 46 inches (Figure 9). Pit P4 was also clearly identified in the composite images derived from 13 different inspection locations at 160 kHz excitation frequency (Figure 10). The signal-to-noise ratio (SNR) for Pit P4 ranged from 8.1 to 29 dB. Guidedwave reliably detected all pits in both mock-ups with the original GWPA sensor design during Phase I testing.

In Phase II, Guidedwave detected P4 from multiple transducer locations at excitation frequencies of 150 and 165 kHz. Pit P4 was identified in the single shot image as seen in Figure 11 and also clearly identified in the composite images derived from eight different inspection locations at 165 kHz excitation frequency (Figure 12). Guidedwave reliably detected all of the pits from Table 2 with the new Hanford-Probe A GWPA sensor.

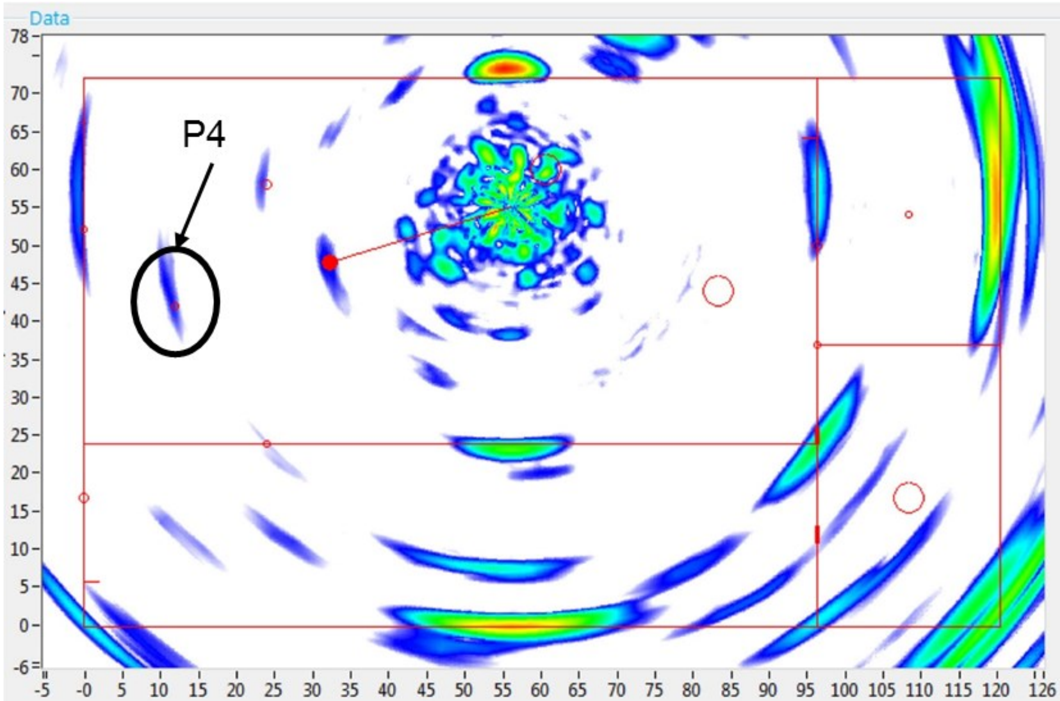

Figure 9. GWPA Scan on the *SET* Mock-up at Location C, Collected at 160 kHz with the Original GWPA Sensor (image from Figure 40 of Appendix A in Moran et al. 2017b)

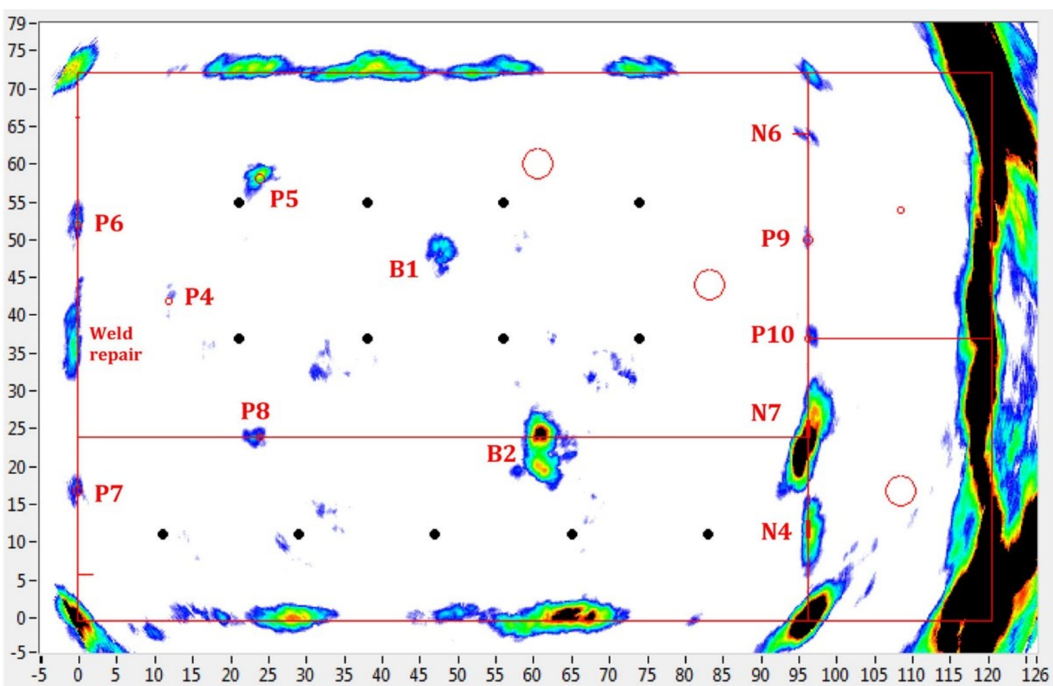

Figure 10. Composite Image from the *SET* Mock-up, Collected From 13 Measurement Locations with the Original GWPA Sensor (Figure 26 of Appendix A in Moran et al. 2017b)

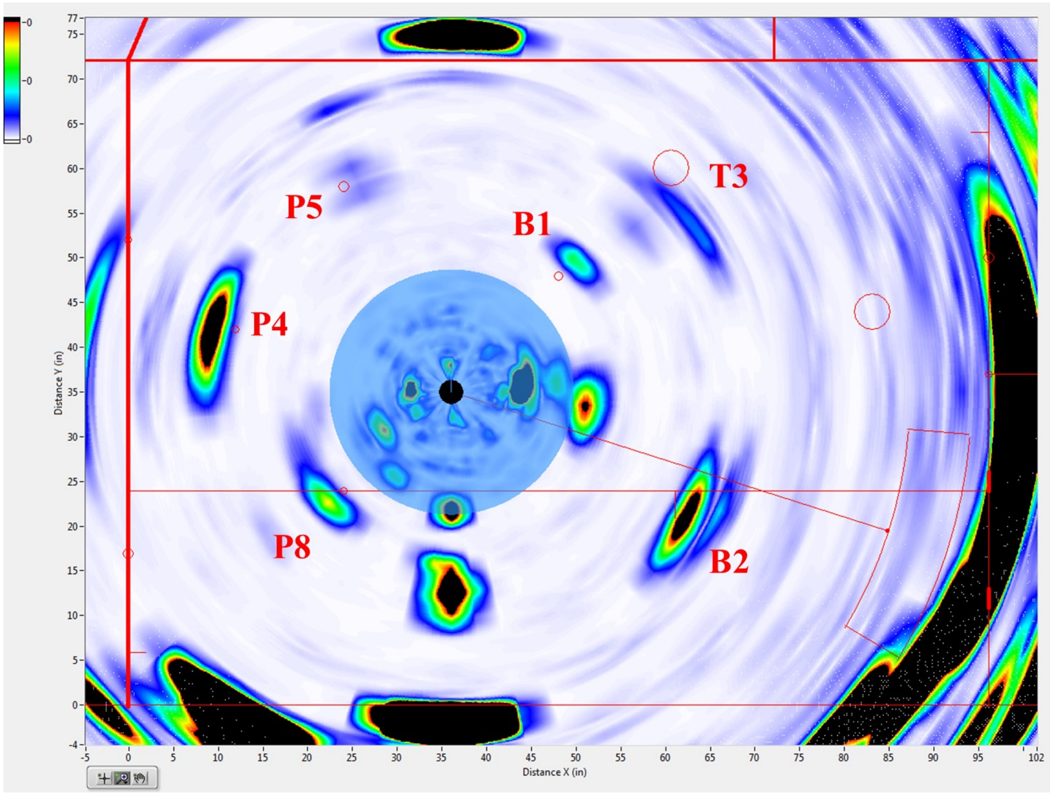

Figure 11. GWPA Scan on the PII Mock-up, Collected at 150 kHz with Hanford-Probe A, Showing Detection of Surrogate Flaws P4, P8, P5, B1, T3, and B2

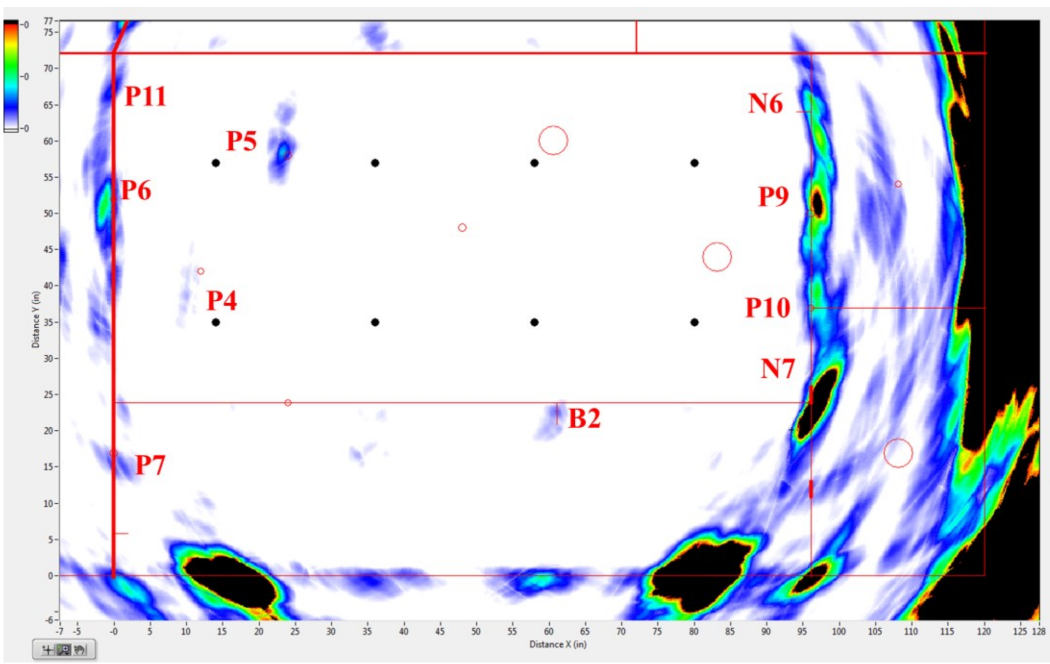

Figure 12. Composite Image from the PII Mock-up, Collected From Eight Measurement Locations with Hanford-Probe A

6.3 Flaw Type – Notch (N4)

Notch N4 is a 2-inch-long, 0.125-inch-wide machined notch with a depth of 50% of the plate thickness (0.250 in.). Notch N4 is located in the 1/2- to 1/2-inch weld of the PII mock-up and oriented parallel to the weld as shown in Figure 13.

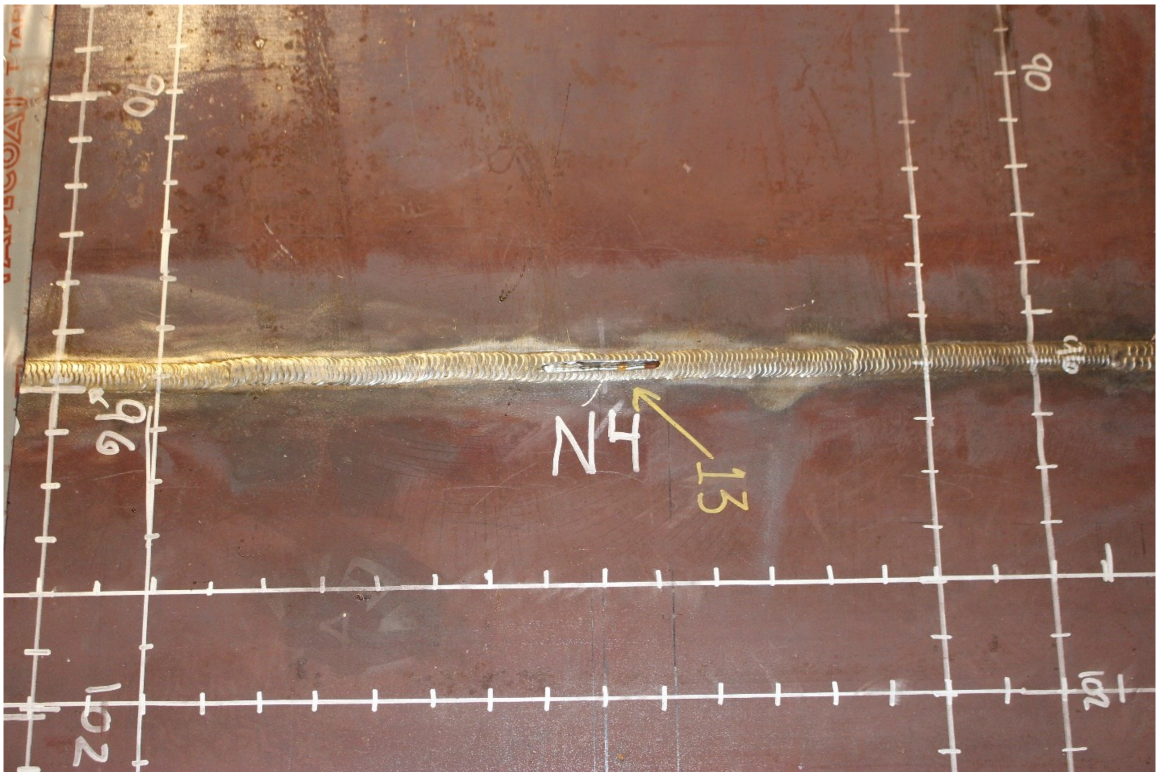

Figure 13. Photograph of Notch N4

Notch N4 was detected during FY 2017 Phase I testing with the original GPWA sensor and by the new GWPA sensor Hanford-Probe A during FY 2018 Phase II testing.

In Phase I, Guidedwave detected N4 from seven different transducer locations using an excitation frequency of 160 kHz. The farthest position Notch N4 was detected from Transducer Location J was 67 inches away (Figure 14). Notch N4 was also detected in the composite images as seen in Figure 10. The SNR for Notch N4 ranged from 17 to 51 dB. Guidedwave reliably detected all notches in both mock-ups with the original GWPA sensor during Phase I testing.

In Phase II, Guidedwave detected N4 from multiple transducer locations at excitation frequencies of 150 and 165 kHz. Notch N4 was also clearly identified in the single shot image at 165 kHz excitation frequency (Figure 15). Guidedwave reliably detected all of the notches from Table 2 with the new Hanford-Probe A GWPA sensor.

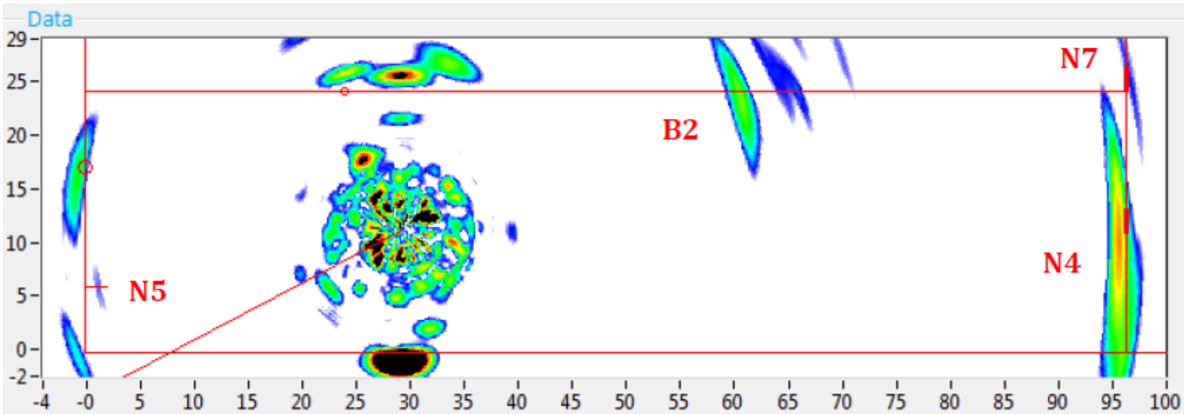

Figure 14. Guidedwave GWPA Scan on the *SET* Mock-up at Location J, Collected at 160 kHz with the Original GWPA Sensor (image from Figure 22 of Appendix A in Moran et al. 2017b)

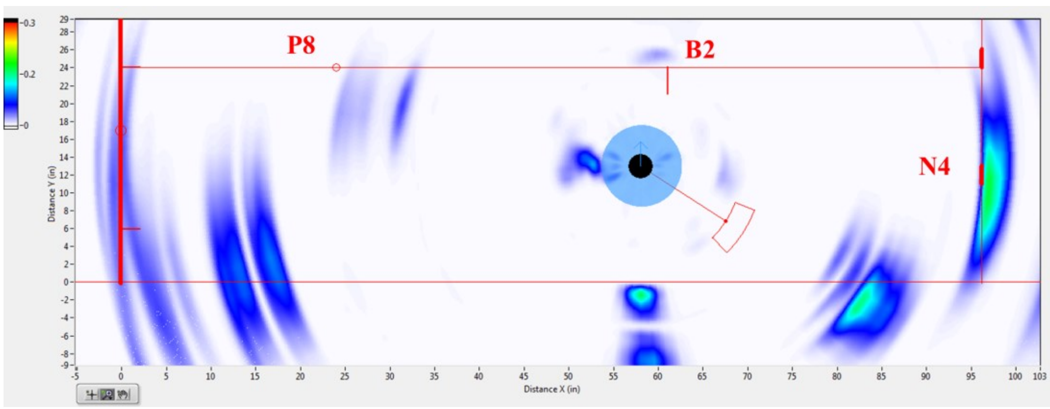

Figure 15. GWPA Scan on the PII Mock-up, Collected at 165 kHz with Hanford-Probe A, Showing Detection of Surrogate Flaws N4, P8, and B2

6.4 Flaw Type – Wall Thinning

Wall Thinning T3 is a 4.0-inch-diameter machined wall thinning with the center depth of 50% of the plate thickness (0.250 in.) located in the base plate of the PII mock-up. A photograph of T3 is shown in Figure 16.

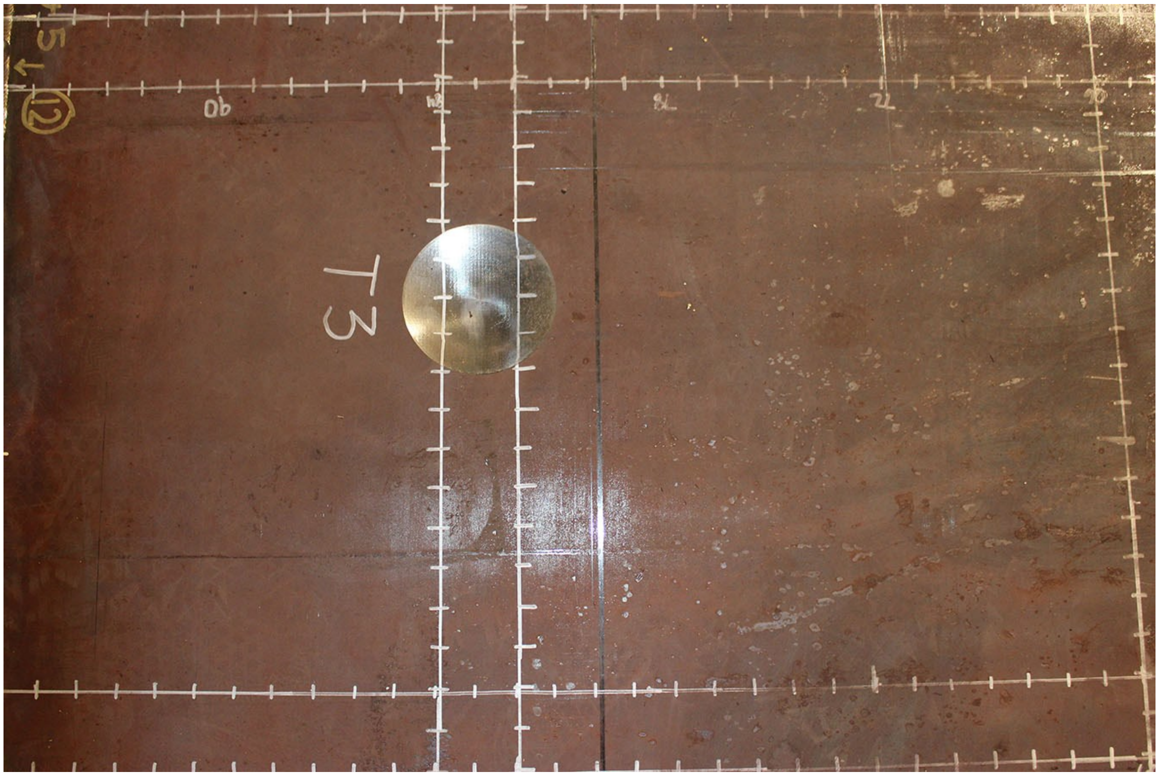

Figure 16. Photograph of Wall Thinning T3

Wall Thinning T3 was detected during FY 2017 Phase I testing and detected by the new GWPA Sensor Hanford-Probe A during FY 2018 Phase II testing.

In Phase I, Guidedwave used the higher frequency version of the GWPA sensor design (shown on the left in Figure 5) pulsed at 225 kHz to detect T3; the flaw was not observed in any of the composite images using the lower frequency GWPA sensor. T3 was detected from two different locations on the 1/2-inch-thick base plate of the PII mock-up using the higher frequency GWPA sensor. Transducer Location II was the farthest from Wall Thinning T3 at 21 inches (Figure 17). The best SNR for T3 was 40 dB. Guidedwave detected both 50% deep wall thinning flaws, but did not detect the 10% or 20% deep wall thinning flaws with the higher frequency GWPA sensor design during Phase I testing.

In Phase II, Guidedwave detected T3 from multiple different transducer locations at excitation frequencies of 165 and 195 kHz. Wall Thinning T3 was clearly identified in the single shot image at an excitation frequency of 195 kHz (Figure 18). Guidedwave reliably detected the one 50% deep wall thinning flaw (T3) but was not able to detect the 10%, 20%, and 50% (T4) deep wall thinning flaws with the Phase II Hanford-Probe A design.

The inability of Hanford-Probe A to detect the 10% or 20% deep wall thinning flaws is consistent with the inability of the original GWPA sensor to detect the same flaws. The primary reasons Hanford-Probe A did not detect the 50% deep wall thinning (T4) are, 1) the ultrasonic reflections from nearby mock-up edges interfere with flaw reflections, which would not be an issue in a real tank, and 2) the sensor standoff distance from the T4 flaw while coupled with the magnetic coupler is nearly the same as the sensor's 10-inch dead zone radius, which precluded detection of the flaw.

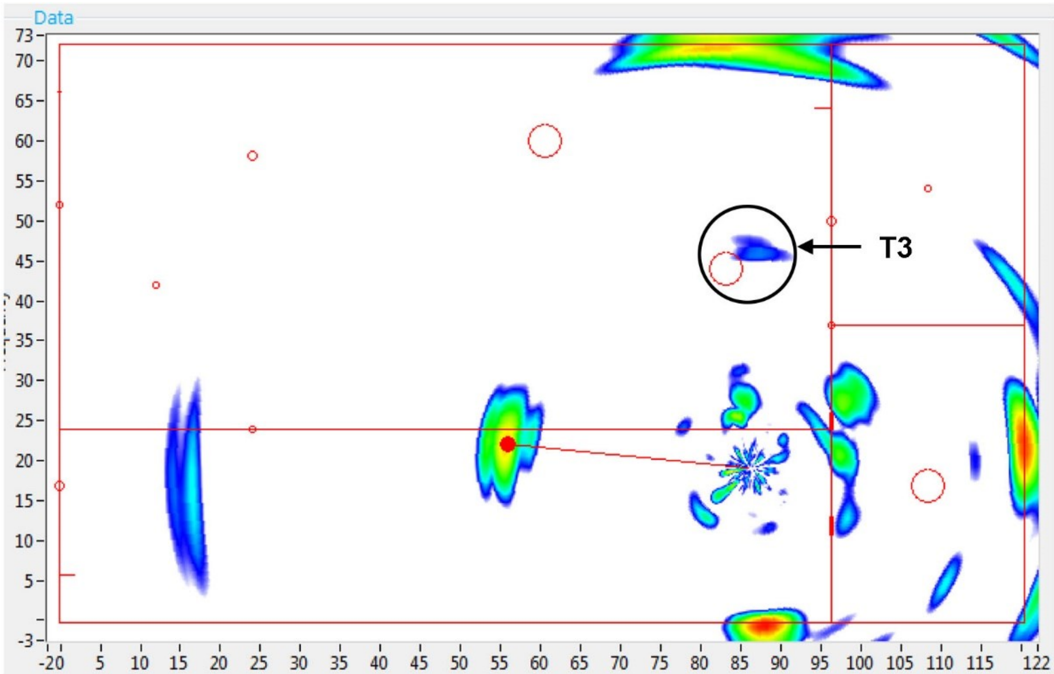

Figure 17. GWPA Scan on the *SET* Mock-up at Location II, Collected at 225 kHz with the Higher Frequency Version of the Original GWPA Sensor Design (image from Figure 64 of Appendix A in Moran et al. 2017b)

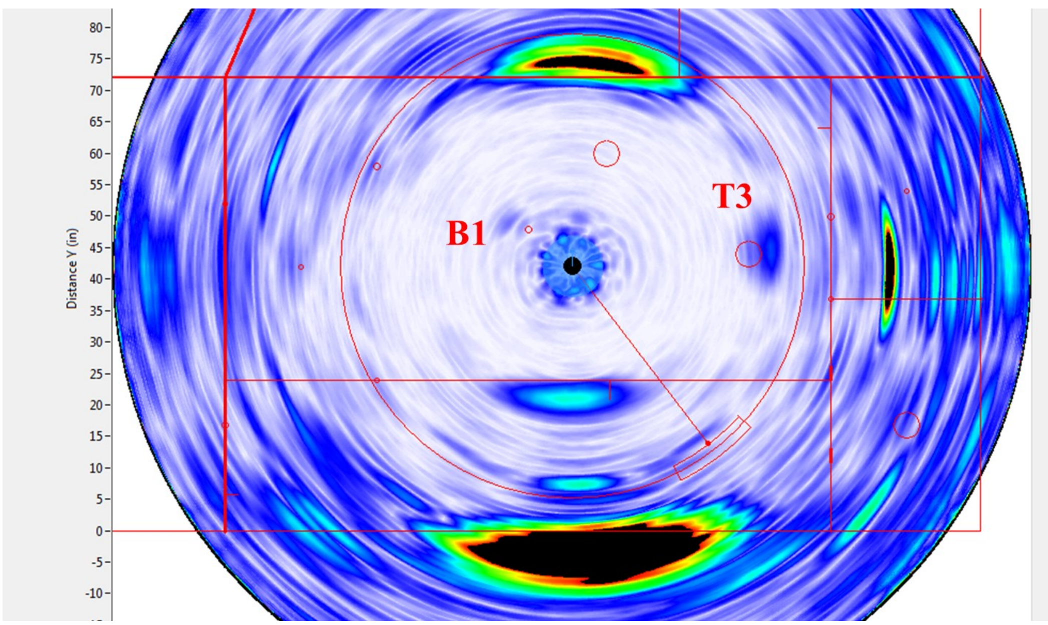

Figure 18. GWPA Scan on the PII Mock-up, Collected at 195 kHz with Hanford-Probe A, Showing Detection of T3 and B1 (suppression filter turned off)

6.5 Testing Challenges

Although detection of the flaws went well, a list of challenges that were observed during testing were identified. Noteworthy observations include the following:

- Hanford-Probe A was received the day before Guidedwave was expected to be at PNNL for testing. The delayed receipt of the sensor did not allow Guidedwave time to perform any preliminary testing of the new sensor or couplant membranes before having to perform testing on the actual mock-ups.
- Hanford-Probe B is still being manufactured by Olympus and was not available for testing.
- Hanford-Probe A was designed to have a center frequency of 150 kHz to produce the desired non-dispersive fundamental SH0 wave mode and prevent the emergence of the undesirable dispersive SH1 wave mode. The as-built center frequency of 180–185 kHz introduced the SH1 wave mode in the mock-up test plates, which caused interference at times with SH0 signals and increased the overall noise level.
- The layout of the piezoceramic element array in Hanford-Probe A was designed to produce sound beams with small side lobes at 150 kHz. The as-built center frequency of 180-15 kHz was less compatible with the array layout and led to larger sound beam side lobes, which contributed to the overall noise level.
- Hanford-Probe A could be forced to operate near 150 kHz to reduce the interfering SH1 wave mode and the sound beam side lobes; however, the lower frequency could only be achieved at the expense of the transmit/receive efficiency and, therefore, signal amplitude. The transmit/receive efficiency is maximized at the center (resonance) frequency of the piezoceramic elements.
- The dry couplant membranes did not provide consistent coupling efficiency, which resulted in decreased signal amplitudes at times. Variation in couplant performance can greatly affect the signal strength and noise levels. The quality of the coupling also drives the size of the dead zone and consequently the stand-off distance required from the flaw.
- The magnetic coupler used to supply coupling force to the sensor was able to supply a force around 100 lbs., but it was noted throughout testing that more coupling force (150+ lbs.) used with the dry couplant membranes would reduce the size of the dead zone and higher-amplitude signals.

7.0 Conclusions

Guidedwave was able to complete the scope of testing outlined for *Maturation Testing: Phase II Capability Testing with Phase I Flaws* to facilitate a flaw detection performance comparison between the new GWPA air-slot sensor design Hanford-Probe A and the original GWPA sensor design demonstrated in FY 2017. The comparison was performed to determine the extent to which GWPA sensor design changes impacted the flaw detection performance upon which selection of the sensor technology was originally based for the purpose of determining whether the flaw detection performance of Hanford-Probe A is at least equal to that of the original GWPA sensor evaluated under Phase I *SET*, or whether design improvements are necessary.

Based on flaw detection ability alone, the flaw detection performance of Hanford-Probe A is considered equivalent to that of the original GWPA sensor demonstrated in FY 2017. The flaw detection performance comparison does not include SNR (signal quality), which was not yet available at the time this report was written. Hanford-Probe A detected all reportable- and actionable-level pits and notches and detected wall thinning at a depth of 50% wall thickness. The new sensor detected flaws that originated from both the top and the bottom surfaces of the plate and detected all flaws in 90-degree weld confluence. As observed previously with the original GWPA sensor, Hanford-Probe A was unable to detect the reportable- or actionable-level surrogate wall thinning flaws.

Hanford-Probe A will fit within the dimensions of the air-slots as outlined in the Phase II requirement document and is capable of flaw detection using a 150-foot-long cable. Hanford-Probe A can also clearly detected the flaws previously mentioned using the dry, shear couplant membranes, which eliminates the need for liquid couplant and any direct contact between the shear couplant and the tank bottom.

There were some challenges noted during testing related to the center frequency of the sensor and different couplant variations, both of which significantly affected the signal amplitude and fidelity throughout testing. Even with the challenges noted, which can be incorporated into the next design as Phase II continues, the flaw detection results from *Maturation Testing: Phase II Capability Testing with Phase I Flaws* show that Hanford-Probe A performed as well as the original Phase I probe with respect to flaw detection.

8.0 Future Work

Maturation Testing: Phase II Capability Testing with Phase I Flaws revealed design improvements that could be incorporated into an updated Hanford-Probe A sensor to achieve an ultrasonic center frequency closer to 150 kHz. The frequency adjustment would likely yield improvements in signal fidelity and SNRs by exciting the desired fundamental SH0 wave mode in the mock-up plates with minimal excitation of the undesired SH1 wave mode; increasing compatibility of the sensor frequency with the element layout to eliminate unwanted sound beam side lobes; and allowing the piezoelectric elements of the sensor to operate at high efficiency during signal transmitting/receiving functions. The dry couplant formulation or methods to increase the uniformity of the material properties and/or thickness of the dry couplant membranes is also recommended to improve coupling. It may be convenient to address the sensor frequency adjustment while making design changes that would allow the sensor to tolerate temperatures closer to what will be experience in the DST and be fastened to the robotic system.

The next steps for air-slot NDE sensor testing include completing Flaw Detection Performance Testing and other testing identified in the Phase II test plan, as warranted based on flaw detection performance, for Hanford-Probe B and preferably a more optimized Hanford-Probe A. Testing to assess the (1) radiation tolerance of vulnerable components for the sensor and (2) the ability of the different prototypes for the robotic sensor-coupling mechanisms responsible for supplying the force needed to couple the GWPA sensor to the primary tank bottom is also to be completed in FY 2018 in collaboration with Washington State University.

During each test of an air-slot NDE sensor or robotic deployment system design element or full assembly, design improvement needs that arise will be documented to ensure they are considered for incorporation into the final sensor or robotic designs prior to sensor/robot integration; for example, sensor design improvements to produce only desired ultrasonic wave modes in tank bottom plates, and robotic sensor coupling mechanism design changes to supply 150+ lbs. of force to the sensor. Once the maturation of air-slot NDE sensors and robotic deployment systems is complete, the sensors and robotic deployment system will be integrated to produce robotic NDE inspection systems for primary tank bottom inspection. A series of laboratory tests and field trials are recommended to identify and address any remaining improvements needed to ensure inspection system reliability during deployment under a DST. Ultimately, the robotic NDE inspection systems will be put through a performance demonstration test to qualify the inspection system, procedures, and personnel for official in-service inspections of primary tank bottoms.

9.0 References

Bandyopadhyay K, S Bush, M Kassir, B Mather, P Shewmon, M Streicher, B Thompson, D van Rooyen and J Weeks. 1997. *Guidelines for Development of Structural Integrity Programs for DOE High-Level Waste Storage Tanks*. BNL-52527, Brookhaven National Laboratory, Upton, New York.

Boomer KD, AJ Feero and JR Gunter. 2016. *Double-Shell Tank Integrity Project Plan*. RPP-7574, Rev. 4, Washington River Protection Solutions, Richland, Washington.

Denslow KM, TL Moran, MR Larche and SW Glass III. 2018a. *NDE Technology Development Program for Non-Visual Volumetric Inspection Technology – Phase I Summary Report*. PNNL-26924, Pacific Northwest National Laboratory, Richland, Washington.

Denslow KM, TL Moran, MR Larche, SW Glass III, CP Baker and SA Bailey. 2018b. *NDE Technology Development Program for Non-Visual Volumetric Inspection Technology Phase II Technical Requirements for Sensor & Robotic Deployment System Maturation*. PNNL-27340 Rev. 0, Pacific Northwest National Laboratory, Richland, Washington.

Garfield JS, BJ Vazquez, JR Gunter, AJ Feero and KD Boomer. 2015. *Double-Shell Tank Integrity Improvement Plan*. RPP-PLAN-57352, Rev. 1, Washington River Protection Solutions, Richland, Washington.

Moran TL, MR Larche, KM Denslow and SW Glass III. 2017a. *NDE Technology Development Program for Non-Visual Volumetric Inspection Technology – Technology Screening Report*. PNNL-26328, Rev. 0, Pacific Northwest National Laboratory, Richland, Washington.

Moran TL, MR Larche, KM Denslow and SW Glass III. 2017b. *NDE Technology Development Program for Non-Visual Volumetric Inspection Technology – Sensor Effectiveness Testing Report*. PNNL-26603, Rev. 0, Pacific Northwest National Laboratory, Richland, Washington.

Pacific Northwest
NATIONAL LABORATORY

www.pnnl.gov

902 Battelle Boulevard
P.O. Box 999
Richland, WA 99352
1-888-375-PNNL (7665)

U.S. DEPARTMENT OF
ENERGY